Journal of Materials Chemistry C

Tuning Charge Carrier Dynamics through Spacer Cation Functionalization in Layered Halide Perovskites: An ab initio Quantum Dynamics Study

Journal:	*Journal of Materials Chemistry C*
Manuscript ID	TC-ART-01-2023-000331.R1
Article Type:	Paper
Date Submitted by the Author:	09-Feb-2023
Complete List of Authors:	Nayak, Pabitra; IIT Delhi Department of Chemistry, Dept. Chemistry Ghosh, Dibyajyoti; IIT Delhi,

Tuning Charge Carrier Dynamics through Spacer Cation Functionalization in Layered Halide Perovskites: An *ab initio* Quantum Dynamics Study

Pabitra Kumar Nayak[1] and Dibyajyoti Ghosh[1,2]

[1]Department of Chemistry, Indian Institute of Technology, Delhi, Hauz Khas, New Delhi-110016, India

[2] Department of Materials Science and Engineering (DMSE), Indian Institute of Technology, Delhi, Hauz Khas, New Delhi-110016, India

Abstract

Dion-Jacobson (DJ) phase two-dimensional (2D) hybrid halide perovskites are promising for environmentally stable optoelectronic device applications due to their attractive photophysical properties, including long charge carrier lifetime and partially suppressed non-radiative losses. However, the atomistic details of the structure-property relationship are severely limited, which substantially restricts the strategic materials designed for these layered halide perovskites (LHPs). Here, we combine nonadiabatic molecular dynamics and time-domain density functional theory to understand the effects of spacer cation functionalization on the ground and excited-state charge carrier dynamics in DJ phase LHPs. Our in-depth study reveals that the fluorination of spacer cations considerably restricts the thermal motions of LHPs at ambient conditions. The compact structure weakens the overall electron-phonon interactions and reduces the thermal fluctuations of band edges in real-time. These dynamic modifications partially mitigate the non-radiative recombination, prolonging the lifetime of photogenerated charge carriers. The suppressed carrier loss mechanism strongly suggests that the fluorinated spacer cation-based LHPs would exhibit enhanced performance as optoelectronic materials. These systematic simulations of excited state carrier dynamics elaborate that chemically viable functionalization of the spacer cations is a robust approach to improve the photophysical properties of 2D halide perovskites strategically. These insights also guide us to propose a few potential strategies to design highly beneficial spacer cations of LHPs that can be introduced in next-generation optoelectronic devices.

Introduction

The two-dimensional (2D) hybrid organic-inorganic layered halide perovskites (LHPs) are engaging significant research interest owing to their exceptional photophysical properties. These materials are utilized as semiconductors in various optoelectronic devices such as solar cells[1–3], light-emitting devices[4–6], and photodetectors[7,8]. The general chemical formula for LHPs is $A'_mA_{n-1}B_nX_{3n+1}$ (m =1 (2) for dicationic (monocationic) spacer A′ ; A is monocation, i.e. methylammonium (MA), Cs; B is dicationic metal, i.e. Pb, Sn; and X are halogens, i.e. I, Br, Cl) where A′ spacers template the inorganic B_nX_{3n+1} slabs (*n* is the number of BX_3 layer). The hydrophobic nature of these organic spacer cations causes the enhanced stability of the layered perovskites at ambient conditions compared to their 3D counterparts.[9–13] However, the wide band gap and poor out-of-plane charge transport across the spacer cation layers strongly affect the optoelectronic performances of layered perovskites.[14–16] The physicochemical properties of spacer cation can give rise to 2D-perovskites of several structural phases such as

Ruddlesden-Popper (RP)[17–19], Dion-Jacobson (DJ)[20–22], and with alternating cation in the interlayer distance (ACI)[1,23]. Among these, the DJ-phase perovskites are emerging as promising candidates for stable optoelectronic device applications.[24,25] In this phase, the spacer cations are dicationic with positively charged terminal groups (mostly ammonium) that anchor the inorganic slabs through non-covalent hydrogen bonds.[26] The strong inorganic-organic interactions and suitable stacking make DJ-phase perovskites compact and thermally stable with short interlayer distances.[27] Furthermore, the opportunity to tune the inorganic layer thickness, molecular structure of A′ cations, and B-metal composition provides a large chemical space for optimizing the optoelectronic performances of these materials.[26,28–30]

The band edges of LHPs are primarily composed of atomic contributions from the B_nX_{3n+1} layer. Thus, the chemical composition and thickness of the inorganic layer dominantly modify the photophysical properties, including band gaps, absorption coefficients, and effective masses of these materials.[31–33] Though the spacer cations do not influence the static electronic structure near the band edges, recent studies demonstrate their important role in the physicochemical properties and overall structural stabilities of layered halide perovskites.[26,27,34] The non-covalent interactions between organic and inorganic layers finetune the extent of distortion in the inorganic layer (B_nX_{3n+1}), which in turn tune the band gap, and effective masses of these semiconductors.[27,35] At ambient conditions, the A′ cations are further dynamically coupled with the thermal motion of B_nX_{3n+1}, substantially impacting the phonon characteristics and electron-phonon interactions.[36,37] These dynamic interactions modify the excited state charge recombination altering the carrier lifetime. Overall, the stronger electron-phonon coupling strength suggests faster non-radiative charge relaxation that affects the optoelectronic performance of these materials. [38–40]

In this regard, the targeted functionalization of spacer cations unlocks viable strategies for finetuning the structural stability and charge carrier dynamics of LHPs at room temperature.[21,30,41,42] Due to similar steric parameters, the substitution of fluorine (Van der Waals radii ~ 147 ps) with hydrogen (radii ~ 110 pm) in spacer cations maintains the overall crystal structure of LHPs without much geometric distortions[43]. The high electronegativity of fluorine can substantially modify the organic-inorganic sublattice coupling through C-F…X (X is halogen), F…π, and hydrogen bonding interactions.[44–46] Furthermore, the large dipole moment in fluorinated spacer cations originates a high dielectric constant, reducing the associated confinement effects in LHPs. These modifications in electrostatics further weaken the exciton bonding strength and promote free-carrier transport.[47–49] On the other hand, the fluoride ion on the surface could also effectively passivate organic cation and anion vacancy by extensive hydrogen bonding, which improves thermal stability and carrier lifetime in perovskite materials.[50,51] Recently, Lv et al. demonstrated that multifluorinated spacer cations improve the photophysical properties of layered perovskites, significantly enhancing the efficiency of fabricated solar cells.[45] The enhanced hydrophobicity due to repulsive interaction between lone pairs in the oxygen of water and fluorine of spacer cations provides robust moisture resistance for LHPs.[52,53] Despite plentiful experimental reports, we still mostly lack an in-depth understanding of the impact of the fluorinated spacer in dynamic structure and charge carrier recombination processes at ambient conditions for LHPs.

We have employed first-principle-based computational models to explore the structure–optoelectronic properties under ambient conditions in our earlier studies.[22,54–57] In the current work, we combine *ab initio* time-dependent density functional theory (DFT) and non-adiabatic

molecular dynamics (NAMD) to investigate the effects of spacer cation functionalization on electronic structure and carrier relaxation processes in (A)PbI_4 where A is 1,4-phenylenedimethanammonium (PhDMA). Comparing 2,3,5,6-tetrafluoro-1,4-phenylenedimethanammonium (4F-PhDMA) and PhDMA-based single layered (n = 1) lead iodide perovskites, we reveal that the structural dynamics at room temperature get considerably suppressed with fluorination. Such modifications considerably slow down the non-radiative carrier recombination process and designate improved photophysical properties of (4F-PhDMA)PbI_4 compared to the PhDMA-based one. Our detailed study points out that the stiffer lattice weakens the electron-phonon interactions and enhances the carrier lifetime of the photo-excited state. The subtle impact of spacer cations on the charge carrier lifetime of LHPs opens up opportunities to strategically functionalize these molecules for improved optoelectronics.

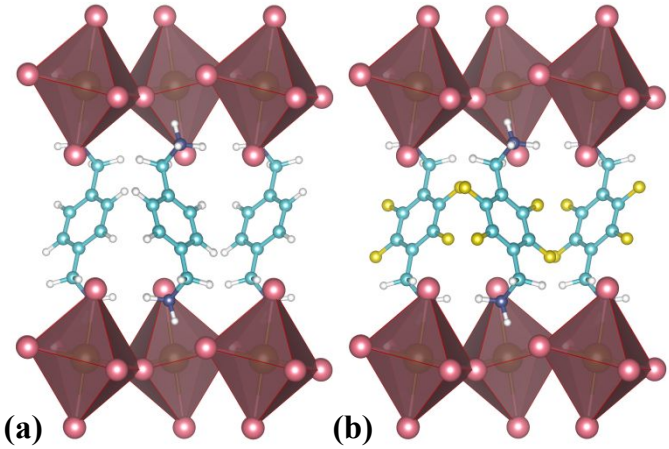

Figure 1: Schematic of optimized structures for (a) (PhDMA)PbI_4 and (b) (4F-PhDMA)PbI_4. The spacer cations PhDMA and 4F-PhDMA stack the inorganic layers formed by corner-sharing PbI_6 octahedra (bronze). Key: iodine, pink; hydrogen, white; carbon, cyan; nitrogen, blue; fluorine, yellow; lead, brown.

Result and Discussion

Static Structural Properties: The computationally optimized geometries of (PhDMA)PbI_4 and (4F-PhDMA)PbI_4 at 0 K exhibit very few differences due to the fluorination of the spacer molecule (Figure S1). In the basic inorganic framework, the PbI_6 octahedra are corner shared through iodide atoms for both the perovskites (Figure 1). The organic molecules are π-stacked in tilted edge-to-face geometry, irrespective of detailed functionalization in PhDMA (Figure S1). As the spacer cations interact with the inorganic layer through non-covalent bonding, the static in-plane Pb-I framework does not alter significantly with fluorination. The details of bond angles, dihedrals, and lengths are tabulated in the Supplementary Information (SI) file (Table S1). Note that, the interlayer I···I distance reduces to some extent for (4F-PhDMA)PbI_4 (6.48 Å) compared to that in (PhDMA)PbI_4 (6.64 Å). The shorter vertical distance between PbI-layers indicates more compact spacer molecule packing that becomes evident while analyzing the structural dynamics in the following sections.

The presence of fluorine atoms in 4F-PhDMA may enhance its non-covalent interaction with PbI-layers in these 2D iodide perovskites.[45,58] For detailed insights, we calculate the non-covalent interactions (NCI) index as introduced by Johnson et al.[59,60] The electron density (ρ)

and its spatial reduced gradients $s(\vec{r})$ are employed to identify and visualize the non-covalent interactions in various solids including halide perovskites.[61–63] The value and sign of $(\lambda_2)\rho$ at the plotted troughs provide the measure for the relative strength of attractive ($\lambda_2 < 0$, blue)/repulsive ($\lambda_2 > 0$, red) interactions, the higher the $|\text{sign}(\lambda_2)\rho|$, the stronger is the interaction (Section S1 in SI for details). The locations of these interactions in real space are also represented by NCI contours. In Figure 2a-b, the reduced density plots exhibit more left-shifted blue troughs in the range of $-0.035 < \text{Sign}(\lambda_2)\rho < -0.02$ for (4F-PhDMA)PbI_4 compared to the PhDMA-based one. The higher negative values of $\text{Sign}(\lambda_2)\rho$ depict the stronger non-covalent interactions between the fluorinated spacer and iodide of the PbI-layer. The 3D-contour plots in Figure 2c-d infer that the attractive non-covalent interactions (blue lobes) are due to the hydrogen bonding between H atoms of the NH_3 head (H_{NH3}) of the PhDMA/4F-PhDMA and axial and equatorial I of the PbI_6 octahedra of the inorganic layer. The moderately shorter H_{NH3}-I distances in (4F-PhDMA)PbI_4 give rise to stronger non-covalent interactions in this perovskite (Table S1). Moreover, with fluorination of the spacer, there are more non-covalent van der Waals interactions through the space between phenyl-ring and PbI-framework cations. The NCI contour between F of 4F-PhDMA and axial iodine atoms (number 1, 4, 5, 8 in Figure 2d and Figure S2) represent the F···I halogen bonding that is unique for (4F-PhDMA)PbI_4. The highly polarizable iodide anion acts as a donor, which gets attracted by electronegative fluorine atoms, forming F···I interactions.[64] These detailed analyses conclude that the presence of fluorine atoms in spacer cations enhances the non-covalent interactions with inorganic layers, boosting the internal stability of layered perovskites. Similar spacer functionalization-induced stability of 2D halide perovskites has been reported by recent experimental works[65,66].

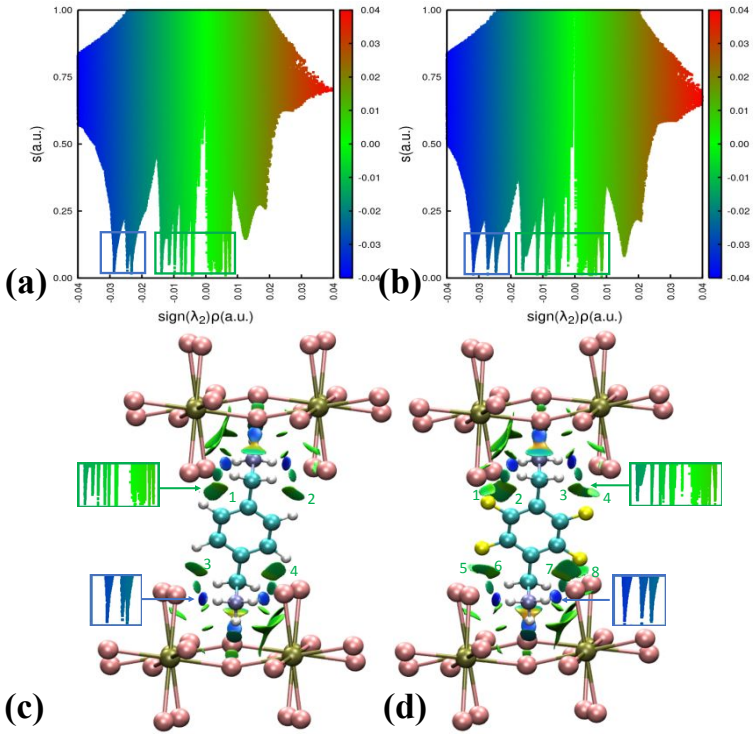

Figure 2: The non-covalent interactions in A′PbI_4. The reduced density gradient ($s(\vec{r})$) plot as a function of $\text{Sign}(\lambda_2)\rho$ for (a) (PhDMA)PbI_4 and (b) (4F-PhDMA)PbI_4. The corresponding 3D isosurfaces (value = 0.3) of s are represented in (c) and (d) with numbers. In (a, b), the troughs in the range $-0.32 < \text{Sign}(\lambda_2)\rho < -0.02$, enclosed with blue boxes, depict the hydrogen bonding

interactions, as also shown with the blue isosurfaces in (c,d). The van der Waals and halogen bonds that are enclosed with light green boxes in (a,b) are numbered and shown in (c, d). Color codes based on sign(λ_2)ρ value -0.04(blue) < 0.0(green) < 0.04(red) have been used for these plots. Attractive and repulsive interaction regions are shown using blue and red isosurfaces, respectively, whereas van der Waals and halogen interactions are presented with green isosurfaces.

Static Electronic Structure: We explore the impacts of fluorination on the static electronic structure of PhDMA-based iodide perovskites. The hybrid functional and spin-orbit coupling included simulations exhibit a direct band gap of 2.07 eV and 2.04 eV for (PhDMA)PbI_4 and (4F-PhDMA)PbI_4, respectively. The minute redshift in the bandgap with fluorinated spacer cations is in good agreement with experimental findings for similar LHPs.[45,48] The electronic charge densities of the VBM and CBM states depict that these are delocalized only over the inorganic PbI frame, as also reported for other similar 2D halide perovskites (Figure S4a-d).[27,37] The VBM and CBM construct from the antibonding overlap of the 6s orbital of Pb and 5p orbital of iodine, and mostly non-bonding 6p orbital of Pb, respectively. (Figure S3a,b , S4a-d) Thus, there is no direct influence of spacer cations on the band edge properties, including the energy gap. As tabulated in Table S1, the negligible change in the PbI-layer geometry with fluorine functionalization of spacers justifies the similar band gaps of A′PbI_4 (A′ = PhDMA, 4F-PhDMA). The plotted band diagrams in Figure S5 represent dominantly direction-dependent band dispersion. The in-plane directions, such as Γ → Z/B, exhibit considerably dispersed energy bands at the band edges. Whereas the out-of-plane direction Γ→ Y shows the non-dispersed flat band at the VBM and CBM. Worth mentioning that, unlike other DJ-phase halide perovskites, the large interlayer I···I distance (> 6Å) prohibits direct electronic interactions between two PbI-layers, resulting in mostly flat bands.[27,67] The calculated effective masses further illustrate the strong anisotropic nature of charge carrier transport in the A′PbI_4 (Table S2). The much smaller in-plane effective masses compared to that along the out-of-plane direction indicate substantially faster carrier transport along the inorganic layers than across the organic layers. As tabulated in Table S2, the lightest holes, and electrons are -0.30 m_e (Γ→ Z) and 0.24 m_e (Γ→ Z) respectively for (PhDMA)PbI_4, and -0.28 m_e (Y→ C) and 0.24 m_e (Γ→ Z) respectively for (4F-PhDMA)PbI_4. Like other static band edge electronic properties, the modification in spacer cations does not influence the band structure and effective carrier masses of A′PbI_4 to any considerable extent. Thus, the static geometries and associated electronic properties are not adequate to elucidate the spacer-dependent optoelectronics of A′PbI_4 perovskites.[45,68]

Dynamic Structure: We perform AIMD simulations for A′PbI_4 (A′ = PhDMA and 4F-PhDMA) at 300 K to capture the structural dynamics in these layered perovskites. The root mean square fluctuations (RMSF) for inorganic lattice sites and organic molecules are included in Figure 3a. The strong influences of spacer cations on the structural dynamics of A′PbI_4 are evident from the RMSF of individual components. For each of the components, fluorination in the spacer considerably lowers the RMSF values, indicating partially restricted atomic motions at ambient conditions (Figure 3a). The root mean square deviation (RMSD), as plotted in Figure S6, also evidently depicts the less dynamic organic and inorganic components for (4F-PhDMA)PbI_4. Fundamentally, the reduced lattice fluctuations point out that the vibrational properties of 2D halide perovskites can indeed be tuned by strategically changing the spacer cation chemistry.

Focusing on the structural dynamics in inorganic layers, we find a narrow distribution of equatorial Pb-I-Pb angles and axial I-Pb-Pb-I dihedral angles over time for (4F-PhDMA)PbI_4 compared to PhDMA-based one (Figure S7a,c). The distributions of I···I interlayer distances are also investigated to reveal the effect of spacer chemistry on the PbI-layer dynamics along the stacking direction (inset of Figure 3b). In Figure 3b, the significantly narrower and shorter I···I distance distribution in (4F-PhDMA)PbI_4 explicitly demonstrates the restricted thermal motion of axial iodides that closely interact with spacer cations. Therefore, the functionalization of spacers substantially impacts the overall dynamics in PbI-layers at 300 K.

The RMSF and RMSD plots in Figure 3a and Figure S6, denote that fluorination reduces the thermal motions of A′ in A′PbI_4 perovskites. To understand the mutual fluctuations in stacked spacer layers, we further plot the distributions of dihedral angles between the two nearest PhDMA/4F-PhDMA. As shown in the inset of Figure 3c, the C-C axis passing through ammonium groups in the benzene ring is considered the molecular axis for these analyses. In Figure 3c, the broad peak for (PhDMA)PbI_4 confirms more thermal fluctuations in the dihedral angles between spacer cations. On the contrary, the dihedrals associated with 4F-PhDMA are distributed over a much narrow range of angles. Such distribution demonstrates a lesser extent of thermal disturbance and strengthened face-to-edge stacked molecular packing for (4F-PhDMA)PbI_4.

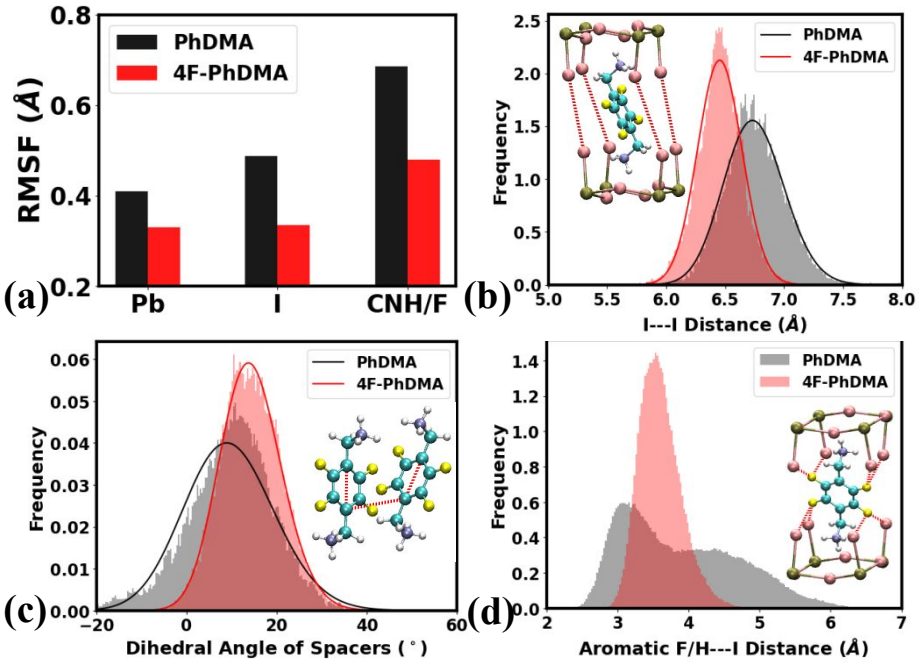

Figure 3. Impact of spacer cations on the structural dynamics in A′PbI_4 at 300 K. (a) Bar chart of root mean square fluctuation (RMSF) value for Pb, I, and spacer cation (CNH/F) for both perovskites. The histogram distribution plots of (b) interlayer distance (terminal I···I distance across spacer cation) between two inorganic perovskite layers, (c) dihedral angle of neighboring spacer cation along molecular C-C axis, and (d) the distance of phenyl ring-attached hydrogen (fluorine) in PhDMA (4F-PhDMA) and terminal iodine of PbI_6 octahedra have been plotted over AIMD-simulated trajectories. The insets of (b-d) represent the schematics of corresponding geometric parameters plotted. The beta functions are used to fit the distribution data in (b) and (c). The wide distribution of H···I distance in (d) does not fit into a beta function.

We further explore the extent of non-covalent interactions that induce dynamic coupling between the inorganic layer and dicationic molecules in these A′PbI_4. The distances between the F/H of the phenyl ring and axial iodide atoms are plotted to find the influence of the fluorinated spacer on the dynamic structural coupling. As shown in Figure 3d, the dynamic F···I distance in (4F-PhDMA)PbI_4 is more narrowly distributed compared to equivalent H···I distributions in (PhDMA)PbI_4. The peak of F···I distribution at 3.54 Å remains close to the sum of van der Waals radii for participating I and F atom pair (3.45 Å), indicating their non-covalent interactions under ambient conditions. Thus, like static structure (Figure 2d), axial iodide atoms mostly retain halogen bonding with fluorine atoms in 4F-PhDMA at 300 K. On the contrary, the lightweight H atoms of PhDMA exhibit a much higher extent of thermal motions, giving rise to widely varied I···H distances (2.5 - 6 Å). The dynamic structure further emphasizes that such I···F interactions restrict the thermal motion of these atoms in (4F-PhDMA)PbI_4. More detailed discussions of these interactions are included in the Supporting Information(SI) Section S2. As plotted in Figure S7(b), the narrowly distributed H_{NH3}···I distance indicates more consistent hydrogen bonding interactions in (4F-PhDMA)PbI_4 compared to PhDMA-based LHP. The stronger hydrogen bonding enhances the internal stability and improves the electronic properties of halide perovskites.[63,69,70] Overall, along with molecular interlayer packing, the dynamic coupling between inorganic and organic moieties is also gets modified with the functionalization of spacer cations. Several studies have reported the complex impact of spacers on the dynamic structure and optoelectronic properties, including charge carrier transport in layered halide perovskites.[22,71–73]

Dynamic Electronic Property: We investigate the influence of structural dynamics on the ground state electronic properties through electron-phonon interactions. At 300 K, the band gap distribution over 5 ps AIMD trajectories for (4F-PhDMA)PbI_4 and (PhDMA)PbI_4 are shown in Figure 4a. These varying band gap values over time exhibit Gaussian distribution largely emphasizing the significant impact of structural dynamics on the basic electronic structure. Moreover, the fitted distribution plot in Figure 4a depicts the wider band gap distribution in (PhDMA)PbI_4 compared to (4F-PhDMA)PbI_4 with a standard deviation of 0.09 and 0.08 eV, respectively. Similar to the band gap, both the VBM and CBM positions are narrowly distributed for (4F-PhDMA)PbI_4 compared to the PhDMA-based one. As shown in Figure 4b, the VBM state gets more affected by thermal fluctuations and has a wider distribution of energy position compared to the CBM state for both systems. The overall band gap and band edge positions dominantly depend on the PbI inorganic framework (Figure S4). More specifically, the equatorial Pb-I-Pb bond angles dominantly influence the electronic structure near the band edges.[63,74,75] As shown in Figure S7(c), the moderately narrow distribution of equatorial Pb-I-Pb angles in (4F-PhDMA)PbI_4 results in its relatively less varied band gap and band edge positions under ambient conditions. Thus, the stiffer lattice of fluorinated spacer cations weakens the electron-phonon interactions, partially suppressing the transient changes in the band edges. The antibonding 6s(Pb)-5p(I) overlap in the VBM causes this band edge to fluctuate more compared to the CBM state that has a dominant contribution of nonbonding 6p(Pb). These analyses explicitly demonstrate that the variation in electronic structures at 300 K can be fine-tuned by strategically choosing spacer cations of 2D layered halide perovskites.

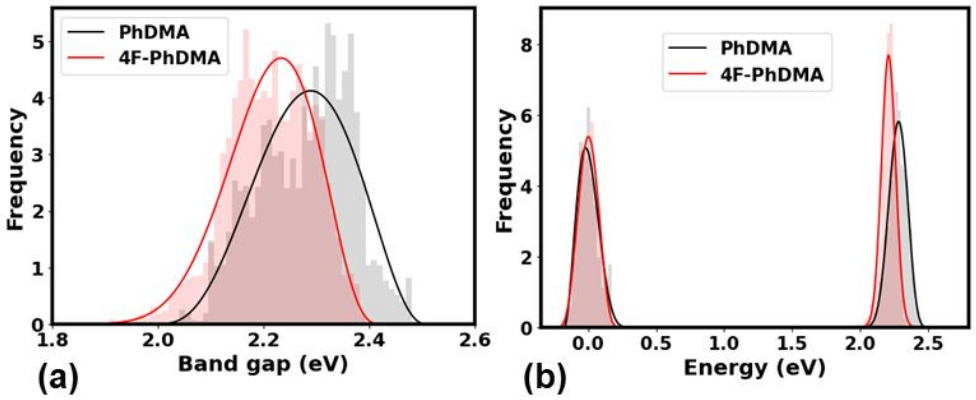

Figure 4. Variation in electronic structures for A′PbI_4 at ambient conditions. (a) The histogram plots for (a) band gaps and (b) the VBM and CBM states along the AIMD trajectories of A′PbI_4 for 5 ps (5000 data points). The narrower distributions of band gap and band edge states for (4F-PhDMA)PbI_4 depict the influence of structural fluctuations on the electronic properties. These electronic structure calculations employ computational inexpensive semi-local functional (GGA-PBE). For (b), the energies of all the electronic states are scaled to the average of the VBM state, which is at E = 0 eV. The beta functions (solid black and red lines) are used to fit the distribution data.

Charge carrier dynamics: The structural fluctuations significantly impact the excited state charge carrier dynamics in halide perovskites.[27,36,57,76,77] However, computational exploration of electron-phonon interactions and their subsequent effects on charge transport is challenging. In that regard, the NAMD with time-domain DFT has emerged as a potential and computationally tractable method to study the non-radiative carrier recombination processes.[78–80] Here, NAMD simulations are used to calculate the change in excited-state charge carrier population over real time in A′PbI_4. In Figure 5a, the non-radiative recombination process of photo-generated carriers is faster for (PhDMA)PbI_4 than for (4F-PhDMA)PbI_4. Employing the short-time linear approximation for the exponentially increasing function, the carrier lifetimes are calculated as 17.8 ns and 29.01 ns for PhDMA and 4F-PhDMA-based layered perovskites, respectively. Hence, the fluorination of spacer cations indeed contributes to realizing a longer carrier lifetime and deaccelerates nonradiative processes that are highly desired for improved efficiency of LHP-based solar cells and LEDs. The evaluated carrier lifetime of the nanosecond scale in these layered halide perovskites is also in good agreement with the experimental reports.[81–83]

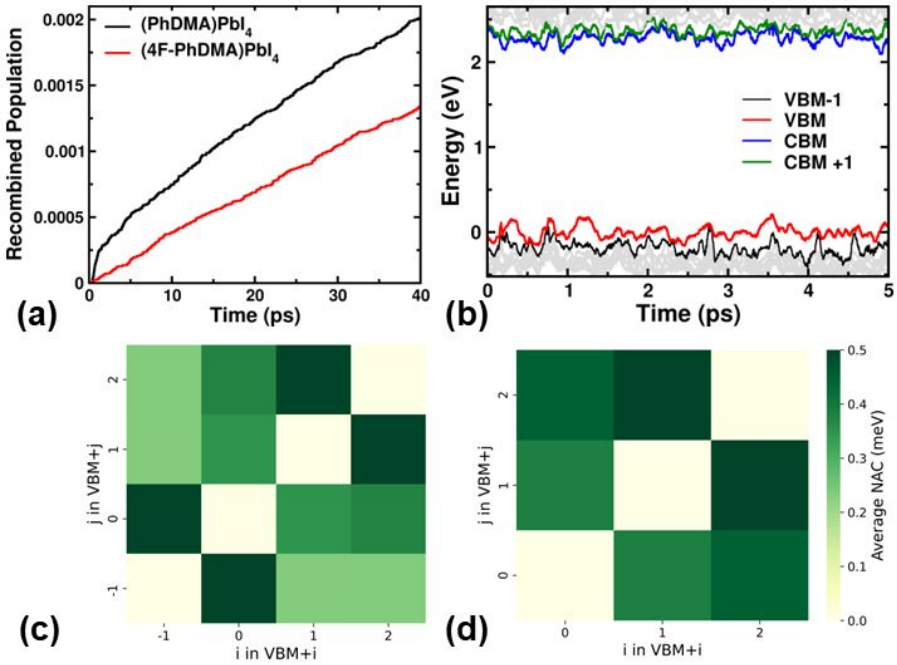

Figure 5. The excited state charge carrier dynamics in A′PbI_4 at 300 K. (a) The population of non-radiatively recombined electron-hole over time in (4F-PhDMA)PbI_4 and (PhDMA)PbI_4. With fluorination in spacer cations, the recombination rate slows down, indicating a longer carrier lifetime. The function $f(t) = 1 - \exp(-t/\tau)$ is used to fit the population rise with time; τ is the electron-hole recombination time. (b) The energy states as a function of time in (PhDMA)PbI_4. Multiple energy states become transiently close to the VBM and CBM due to thermal fluctuations in the lattice. The time-averaged absolute NACs between energy states ranged from (c) VBM-1 to CBM+1 for (PhDMA)PbI_4 and (d) VBM to CBM+1 for (4F-PhDMA)PbI_4. i = 0 and i = 1 are the VBM and CBM states, respectively. The uniform scale for the heatmap considered for (c, d) is presented on the right of (d).

Several intrinsic properties, such as electronic band gap variation, electron-phonon coupling induced non-adiabatic transitions, and quantum decoherence, substantially impact the carrier dynamics in LHPs.[36,84,85] We further explore these key factors for an atomistic understanding of the relationship between structural distortion and excited state charge carrier dynamics. Both elastic and inelastic carrier scattering processes are active at ambient conditions in halide perovskites.[77,86,87] In the inelastic pathway, the electronic and phononic subsystems exchange the excess energy that originates due to initial photoexcitation. During non-radiative recombination, this extra energy of excited electrons gets dissipated to the phonon modes of perovskite lattice, and electron-hole recombines producing heat in the system.[88] The extent of this inelastic electron-phonon interaction is quantified by calculating nonadiabatic coupling (NAC) strength over the simulation time.[89,90] Generally, the high time-averaged NAC values for the participating pair of states (VBM and CBM for this case) signify the strong inelastic electron-phonon couplings and, consequently, fast non-radiative charge recombination process across the electronic band gap.[91,92] Additionally, a greater number of closely spaced energy eigenstates (energy window of ~50 meV) to the band edges can actively participate in the charge carrier relaxation process in real-time, accelerating the non-radiative recombination.[93] In this regard, we find that the Kohn-Sham states VBM-1 and CBM +1, along with the VBM and CBM, can participate in the electron-hole recombination process for

(PhDMA)PbI_4 (Figure 5b). Whereas, the VBM, CBM, and CBM+1 states actively participate in such process for (4F-PhDMA)PbI_4 (Figure S8). The strong thermal fluctuation of the VBM-1 state results in its possible participation only in PhDMA-based perovskites. The calculated NACs between all active states are included in Table S3. The very similar NAC strengths between VBM-CBM states for both LHPs indicate that other key factors cause the difference in calculated carrier relaxation rates (Figure 5a). Further analyses depict that the involvement of dynamic VBM-1 state in the inter-band carrier relaxation process and considerably strong NAC with conduction band states opens more non-radiative channels, resulting in faster recombination in (PhDMA)PbI_4. The fluctuations of the Kohn-Sham energy states over time are closely related to the structural dynamics of atoms that contribute to the wave function of those states. The VBM and VBM-1 states have the dominant contribution from I(5p) and Pb(6s) in these layered perovskites. The RMSF analyses in Figure 3a depict that PhDMA-based perovskite has a more dynamic Pb/I framework compared to (4F-PhDMA)PbI_4. As discussed, weakly packed PhDMA dications introduce more thermal fluctuations into the inorganic lattice, which in turn involve more energy states in carrier relaxation processes, accelerating the non-radiative recombination process.

Influence Spectra: Exploring the electron-phonon interaction further, we evaluate the influence spectra for PhDMA and 4F-PhDMA-based iodide perovskites. The unnormalized autocorrelation function of the electronic bandgaps over time is Fourier transformed to simulate these spectra.[89] The phonon modes that actively couple to electronic structure and participate in electron-hole recombination can be identified from the peak positions of these spectra. In Figure 6a, the active phonon modes for electron-phonon interaction appear in the low-frequency region, <300 cm^{-1}. This characteristic of influence spectra has also been reported for other similar layered perovskites.[27,37,38,92,94] Note that the high-frequency modes associated with the stretching and bending of bonds in organic cations do not directly participate in carrier recombination processes. The band edge charge densities also point out the absence of the electronic contribution of spacer cations to those states (Figure S4). However, the apparent difference in spectra for (4F-PhDMA)PbI_4 and (PhDMA)PbI_4 indicate that spacer cations do influence the excited-state carrier dynamics incidentally. The dominant peaks below 100-140 cm^{-1} are attributed to the stretching, bending, and octahedral rocking/twisting of the inorganic Pb-I framework that contains heavy and slow atoms.[95] The higher frequencies at 140-300 cm^{-1} are associated with the dynamic interaction between the inorganic cage and spacer cation.[96–98] In this range, more dynamic (PhDMA)PbI_4 exhibits prominent peaks indicating the opening of added channels for non-radiative electron-phonon relaxation. The stronger thermal fluctuations in spacer cations, as shown in Figure 3a,c, originate considerable distortions in the inorganic PbI structure, influencing the time evolution of band edge wave functions. Thus, the involvement of higher phonon modes in the carrier relaxation process is one of the key reasons for faster electron-hole recombination in (PhDMA)PbI_4. The spectral function calculated for other involved electronic states near the band edges also depicts very similar characteristics, where PhDMA-based perovskite involves more phonon modes for carrier relaxation (Figure S9a,b). These atomistic investigations emphasize that the fluorination of spacers suppresses the overall dynamic fluctuations of lattice, weakening the electron-phonon interactions and subsequently slowing down the recombination processes.

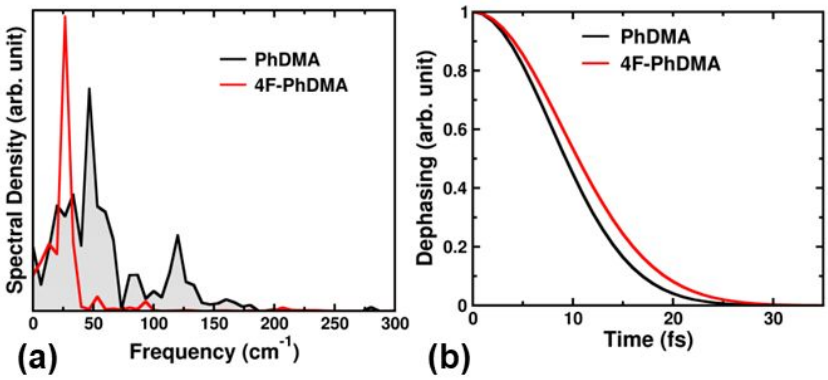

Figure 6. The electron-phonon interactions and dephasing processes in A′PbI_4 at 300 K. (a) The Fourier transform of autocorrelation functions for the band gap fluctuations and (b) pure-dephasing functions for the VBM-CBM transition in (PhDMA)PbI_4 and (4F-PhDMA)PbI_4. The appearance of a broader range of frequencies in (a) indicates a greater number of active phonon modes interacting with the dynamic electronic structure of PhDMA-based lead iodide perovskite. The y-axis scale is consistent but in arbitrary units.

Dephasing Process: The nonadiabatic coupling between two energy states in real-time introduces quantum transition by forming wavefunction superposition. The elastic electron-phonon interactions suppress the quantum coherence and destroy the superposition between involved electronic states.[99–101] This leads to the collapse of wavefunction to one of the states, restraining the associated transition probability. In our study, faster decoherence between band edge states would enhance the electron-hole recombination time. The quantum decoherence in solids typically occurs in tens of femtoseconds (fs), much faster than the electro-hole recombination times, indicating the necessary incorporation of this effect during the carrier relaxation simulations (Figure 6b). As detailed elsewhere, the decoherence time can be evaluated as pure-dephasing time employing linear response formalism.[102,103] The calculated decoherence time for PhDMA and 4F-PhDMA-based perovskites are 7.9 fs and 8.9 fs, respectively. Very similar pure-dephasing times point out the insignificant influence of the decoherence process on the distinctly different carrier relaxation times in these LHPs, as observed experimentally and computed here (Figure 5a).

Exploring all the influencing factors, we find that the non-radiative carrier recombination rate has a complex relationship with electronic and vibrational properties in LHPs. According to Fermi's golden rule, the magnitude of the energy gap between two states inversely affects the electron-hole recombination rate that involves those energy states.[104] The rate also depends on the square of the NAC strength, which represents the transition probability.[105] As the time-averaged band gaps of (PhDMA)PbI_4 and (4F-PhDMA)PbI_4 are scarcely different (Figure 4a and Table S2), the dominant factor emerges to be the NAC among the involved valence band and conduction band states in the recombination process. The higher NAC strengths and a greater number of involved phonon modes originate the faster electron-hole recombination rate across the band gap in PhDMA-based iodide perovskite. On the contrary, the fluorinated spacer cations exhibit stronger inter- and intralayer non-covalent interactions suppressing the dynamic fluctuations in (4F-PhDMA)PbI_4. Such modifications in vibrational properties weaken the electron-phonon interactions, leading to a reduced non-radiative charge recombination rate.

Conclusion

To conclude, we combine time-domain DFT and NAMD simulations for understanding the impact of dynamic structure on real-time excited state carrier evolution in LHPs. The study emphasizes the key role of spacer cation dynamics on the photoinduced charge carrier motion. The considered DJ-phase perovskites are identical in chemical composition ($APbI_4$) except for the spacer cations. Thorough NCI analyses reveal that fluorination enhances the non-covalent interactions between the spacer and PbI-framework. The compact spacer layer stacking, along with the halogen bond between terminal iodides and fluorine atoms of 4F-PhDMA, contributes to the non-covalent bonding. These spacer-induced structural modifications partially suppress the overall lattice fluctuations in (4F-PhDMA)PbI_4 at ambient conditions. The reduced distortions in the PbI framework further result in narrower distribution of band gaps and band edge positions over time for 4F-PhDMA-based perovskite compared to that for (PhDMA)PbI_4. Exploring photoinduced excited carrier dynamics, NAMD simulations exhibit the slower nonradiative electron-hole recombination rate for (4F-PhDMA)PbI_4. Under ambient conditions, the greater extent of structural motion in (PhDMA)PbI_4 involves additional energy states and activates multiple phonon modes for nonradiative carrier relaxation across the bandgap. These factors consequently introduce additional non-adiabatic channels for the recombination process, resulting in faster decay in excited state carrier populations. The longer carrier lifetime for layered perovskites with fluorinated spacer cations strongly indicates its improved efficiency as a variety of optoelectronic devices, including solar cells and light-emitting diodes.

Our study represents an atomistic insight into excited state charge carrier dynamics under ambient conditions, providing a detailed understanding of the relationship between structural dynamics and carrier recombination processes. We find that the charge carrier dynamics can be substantially tuned by strategically modifying the functional groups of spacer cations in 2D-perovskites. Furthermore, the standard protocol for functionalizing commonly used organic spacer molecules with a variety of chemical groups is widely known. Thus, computational insights on the impact of functionalized spacers on photophysical properties can guide its experimental design for high-efficiency optoelectronic devices. The importance of enhanced structural rigidity also indicates other promising choices for spacer cations that may contain larger π-cloud (naphthalene), and electrostatically active heteroatoms (N, O-heterocycles). In the future, a screening of a wide variety of spacers imposing several geometric and electronic criteria as revealed by *in-silico* investigations would greatly help to realize optimized 2D-halide perovskites for several applications.

Computational Methods

The Vienna Ab Initio Simulation Package (VASP) has been used for density functional theory (DFT) calculations and *ab initio* molecular dynamics (AIMD) simulations[106,107]. For all static DFT computations, the projected augmented wave (PAW) approach with a plane-wave basis set and a cut-off energy of 420 eV has been considered.[108,109] For exchange and correlation interactions, the Perdew-Burke-Erzerhof (PBE) functional within semilocal generalized gradient approximation (GGA) has been employed for geometry optimizations and AIMD simulations[110]. During internal geometry optimizations without any constraints, the interatomic forces are relaxed to less than 0.01 $eVÅ^{-1}$. We include dispersion correction DFT-D3 as prescribed by Grimme et al.[111] and used a Γ-cantered 1×4×4 Monkhorst-Pack[112] mesh for these

simulations. For calculating the electronic structures with reasonable accuracy, the spin-orbit coupling (SOC) effects and screened hybrid functionals of Heyd–Scuseria–Ernzerhof (HSE06) were considered. Moreover, the static structural parameter calculations (Table S1) have been done using VESTA software[113].

The hybrid quantum-classical NAMD simulations with the decoherence-induced surface hopping (DISH) method have been used to investigate the charge-carrier dynamics at excited states.[90,114] This approach treats electrons and nuclei as semi-classically and quantum-mechanically, respectively. The such computational method has been successfully applied in the past by some of us and others to compute the excited-state dynamics of inorganic and hybrid perovskites.[22,115] For AIMD simulations, we build a 1×2×2 (8 formula units, total 232 atoms) supercell and employed 1×2×2 Monkhorst-Pack k-point mesh, a time step of 1 fs, and a plane-wave energy cutoff of 400 eV. The DFT-D3 corrections and PBE-GGA exchange-correlation functionals were considered for these calculations since the use of the HSE06 functional is prohibitively expensive here. In this regard, the self-interaction-corrected-DFT emerges as a computationally cheaper and adequately accurate method, which can certainly be an affordable choice for future studies of a similar kind.[116–118] For AIMD, we initiate the simulations considering DFT optimized structure, which is then heated to 300 K via repeated velocity rescaling for 4 ps. To guarantee the thermal equilibrium, additional 4 ps trajectories were produced employing the canonical ensemble. Finally, we generated 10 ps of trajectories under the microcanonical ensemble and used 5 ps of those for the nonadiabatic coupling calculations that are performed at Γ-point. To compute the electron-hole recombination process using the PYXAID code, we consider all 5000 geometries along the trajectories and simulate 500 stochastic realizations of the DISH process for each geometry.[119,120] To make the computation feasible, the non-adiabatic Hamiltonian that we compute for the 5 ps trajectory is iterated several times to achieve the charge recombination dynamics occurring at a much longer timescale. We evaluate the estimated decoherence time as the pure-dephasing time that is formulated in the optical response theory and implemented in PYXAID.[121] In this formulation, the pure-dephasing function is defined under second-order cumulant approximation, $D_{ij}(t) = Exp\left[-\frac{1}{\hbar^2}\int_0^t dt' \int_0^{t'} dt'' \, C_{ij}(t'')\right]$ where C(t) is the unnormalized autocorrelation function (u-ACF), defined as $C_{ij}(t) = \langle \delta E_{ij}(t)\delta E_{ij}(0) \rangle$, $\delta E_{ij}(t) = E_{ij}(t) - \langle E_{ij} \rangle$ is the fluctuation of energy gap between i and jth states from the canonical ensemble average value. [122,123] Due to considerably large computational expenses, we ignore the effect of SOC though it can have a systematic influence on the non-radiative charge recombination process.[124] Furthermore, the exclusion of excitonic effects during our simulations of LHPs is also another noteworthy approximation. The time-dependent Bethe-Salpeter theory for dynamic lattices, which is an important current topic of research, is necessary for the proper inclusion of these effects. However, such approaches still need to be fully developed and implemented numerically.

Conflicts of interest

There are no conflicts to declare.

Acknowledgments

The authors would like to acknowledge the IIT Delhi SEED Grant (PLN12/04MS) and the IIT Delhi HPC facility for computational resources. This work was performed, in part, at the Center for Integrated Nanotechnologies, an Office of Science User Facility operated for the U.S.

Department of Energy (DOE) Office of Science by Los Alamos National Laboratory (Contract 89233218CNA000001) and Sandia National Laboratories (Contract DE-NA-0003525).

References

1 Y. Zhang and N. G. Park, *ACS Energy Lett*, 2022, **7**, 757–765.

2 J. W. Lee, Z. Dai, T. H. Han, C. Choi, S. Y. Chang, S. J. Lee, N. de Marco, H. Zhao, P. Sun, Y. Huang and Y. Yang, *Nature Communications 2018 9:1*, 2018, **9**, 1–10.

3 Z. Wang, Q. Lin, F. P. Chmiel, N. Sakai, L. M. Herz and H. J. Snaith, *Nature Energy 2017 2:9*, 2017, **2**, 1–10.

4 L. Zhang, C. Sun, T. He, Y. Jiang, J. Wei, Y. Huang and M. Yuan, *Light Sci Appl*, 2021, 10.

5 C. Sun, Y. Jiang, M. Cui, L. Qiao, J. Wei, Y. Huang, L. Zhang, T. He, S. Li, H. Y. Hsu, C. Qin, R. Long and M. Yuan, *Nature Communications 2021 12:1*, 2021, **12**, 1–11.

6 Y. Jiang, C. Qin, M. Cui, T. He, K. Liu, Y. Huang, M. Luo, L. Zhang, H. Xu, S. Li, J. Wei, Z. Liu, H. Wang, G. H. Kim, M. Yuan and J. Chen, *Nature Communications 2019 10:1*, 2019, **10**, 1–9.

7 K. Wang, C. Wu, D. Yang, Y. Jiang and S. Priya, *ACS Nano*, 2018, **12**, 4919–4929.

8 J. Feng, C. Gong, H. Gao, W. Wen, Y. Gong, X. Jiang, B. Zhang, Y. Wu, Y. Wu, H. Fu, L. Jiang and X. Zhang, *Nat Electron*, 2018, **1**, 404–410.

9 M. Yuan, L. N. Quan, R. Comin, G. Walters, R. Sabatini, O. Voznyy, S. Hoogland, Y. Zhao, E. M. Beauregard, P. Kanjanaboos, Z. Lu, D. H. Kim and E. H. Sargent, *Nat Nanotechnol*, 2016, **11**, 872–877.

10 M. D. Smith, B. A. Connor and H. I. Karunadasa, *Chem Rev*, 2019, 119, 3104–3139.

11 I. C. Smith, E. T. Hoke, D. Solis-Ibarra, M. D. McGehee and H. I. Karunadasa, *Angewandte Chemie - International Edition*, 2014, **53**, 11232–11235.

12 A. Z. Chen, M. Shiu, J. H. Ma, M. R. Alpert, D. Zhang, B. J. Foley, D. M. Smilgies, S. H. Lee and J. J. Choi, *Nature Communications 2018 9:1*, 2018, **9**, 1–7.

13 Y. Hu, T. Qiu, F. Bai, W. Ruan and S. Zhang, *Adv Energy Mater*, 2018, **8**, 1703620.

14 L. Etgar, *Energy Environ Sci*, 2018, **11**, 234–242.

15 J. C. Blancon, A. v. Stier, H. Tsai, W. Nie, C. C. Stoumpos, B. Traoré, L. Pedesseau, M. Kepenekian, F. Katsutani, G. T. Noe, J. Kono, S. Tretiak, S. A. Crooker, C. Katan, M. G. Kanatzidis, J. J. Crochet, J. Even and A. D. Mohite, *Nature Communications 2018 9:1*, 2018, **9**, 1–10.

16 J. Hu, L. Yan, W. You, J. Hu, L. Yan and W. You, *Advanced Materials*, 2018, **30**, 1802041.

17 H. Tsai, W. Nie, J. C. Blancon, C. C. Stoumpos, R. Asadpour, B. Harutyunyan, A. J. Neukirch, R. Verduzco, J. J. Crochet, S. Tretiak, L. Pedesseau, J. Even, M. A. Alam, G. Gupta, J. Lou, P. M. Ajayan, M. J. Bedzyk, M. G. Kanatzidis and A. D. Mohite, *Nature*, 2016, **536**, 312–317.

18 C. Liang, H. Gu, Y. Xia, Z. Wang, X. Liu, J. Xia, S. Zuo, Y. Hu, X. Gao, W. Hui, L. Chao, T. Niu, M. Fang, H. Lu, H. Dong, H. Yu, S. Chen, X. Ran, L. Song, B. Li, J. Zhang, Y. Peng, G. Shao, J. Wang, Y. Chen, G. Xing and W. Huang, *Nat Energy*, 2021, **6**, 38–45.

19 P. Vashishtha, M. Ng, S. B. Shivarudraiah and J. E. Halpert, *Chemistry of Materials*, 2019, **31**, 83–89.

20 I. H. Park, Q. Zhang, K. C. Kwon, Z. Zhu, W. Yu, K. Leng, D. Giovanni, H. S. Choi, I. Abdelwahab, Q. H. Xu, T. C. Sum and K. P. Loh, *J Am Chem Soc*, 2019, **141**, 15972–15976.

21 B. el Cohen, T. Binyamin, T. Ben-Tzvi, O. Goldberg, A. Schlesinger, I. Balberg, O. Millo, E. Gross, D. Azulay and L. Etgar, *ACS Energy Lett*, 2022, **7**, 217–225.

22 D. Ghosh, D. Acharya, L. Pedesseau, C. Katan, J. Even, S. Tretiak and A. J. Neukirch, *J Mater Chem A Mater*, 2020, **8**, 22009–22022.

23 Y. Zhang, P. Wang, M. C. Tang, D. Barrit, W. Ke, J. Liu, T. Luo, Y. Liu, T. Niu, D. M. Smilgies, Z. Yang, Z. Liu, S. Jin, M. G. Kanatzidis, A. Amassian, S. F. Liu and K. Zhao, *J Am Chem Soc*, 2019, **141**, 2684–2694.

24 T. Niu, Q. Xue and H. L. Yip, *Nanophotonics*, 2021, 10, 2069–2102.

25 C. Ma, D. Shen, T.-W. Ng, M.-F. Lo, C.-S. Lee, C. Q. Ma, D. Shen, T.-W. Ng, M.-F. Lo and C.-S. Lee, *Advanced Materials*, 2018, **30**, 1800710.

26 X. Li, J. M. Hoffman and M. G. Kanatzidis, *Chem Rev*, 2021, 121, 2230–2291.

27 D. Ghosh, D. Acharya, L. Pedesseau, C. Katan, J. Even, S. Tretiak and A. J. Neukirch, *J Mater Chem A Mater*, 2020, **8**, 22009–22022.

28 L. Mao, C. C. Stoumpos and M. G. Kanatzidis, *J Am Chem Soc*, 2019, **141**, 1171–1190.

29 J. C. Blancon, J. Even, C. C. Stoumpos, M. G. Kanatzidis and A. D. Mohite, *Nat Nanotechnol*, 2020, 15, 969–985.

30 J. Hu, I. W. H. Oswald, S. J. Stuard, M. M. Nahid, N. Zhou, O. F. Williams, Z. Guo, L. Yan, H. Hu, Z. Chen, X. Xiao, Y. Lin, Z. Yang, J. Huang, A. M. Moran, H. Ade, J. R. Neilson and W. You, *Nature Communications 2019 10:1*, 2019, **10**, 1–11.

31 J. S. Manser, J. A. Christians and P. v. Kamat, *Chem Rev*, 2016, 116, 12956–13008.

32 L. Mao, W. Ke, L. Pedesseau, Y. Wu, C. Katan, J. Even, M. R. Wasielewski, C. C. Stoumpos and M. G. Kanatzidis, *J Am Chem Soc*, 2018, **140**, 3775–3783.

33 S. Ahmad, P. Fu, S. Yu, Q. Yang, X. Liu, X. Wang, X. Wang, X. Guo and C. Li, *Joule*, 2019, **3**, 794–806.

34 J. Leveillee, C. Katan, J. Even, D. Ghosh, W. Nie, A. D. Mohite, S. Tretiak, A. Schleife and A. J. Neukirch, *Nano Lett*, 2019, **19**, 8732–8740.

35 F. Thouin, D. A. Valverde-Chávez, C. Quarti, D. Cortecchia, I. Bargigia, D. Beljonne, A. Petrozza, C. Silva and A. R. Srimath Kandada, *Nat Mater*, 2019, **18**, 349–356.

36 X. Gong, O. Voznyy, A. Jain, W. Liu, R. Sabatini, Z. Piontkowski, G. Walters, G. Bappi, S. Nokhrin, O. Bushuyev, M. Yuan, R. Comin, D. McCamant, S. O. Kelley and E. H. Sargent, *Nat Mater*, 2018, **17**, 550–556.

37 D. Ghosh, A. J. Neukirch and S. Tretiak, *Journal of Physical Chemistry Letters*, 2020, **11**, 2955–2964.

38 Z. Zhang, W. H. Fang, M. v. Tokina, R. Long and O. v. Prezhdo, *Nano Lett*, 2018, **18**, 2459–2466.

39 Z. Zhang, W. H. Fang, R. Long and O. v. Prezhdo, *J Am Chem Soc*, 2019, **141**, 15557–15566.

40 K. Abdel-Baki, F. Boitier, H. Diab, G. Lanty, K. Jemli, F. Lédée, D. Garrot, E. Deleporte and J. S. Lauret, *J Appl Phys*, 2016, **119**, 064301.

41 H. Yao, Z. Li, G. Peng, Y. Lei, Q. Wang, Z. Ci and Z. Jin, *ACS Appl Mater Interfaces*, 2022, **14**, 35780–35788.

42 G. Yan, G. Sui, W. Chen, K. Su, Y. Feng and B. Zhang, *Chemistry of Materials*, 2022, **34**, 3346–3356.

43 G. Mohanty, A. Sebastian, H. S, K. N. Parida and I. Neogi, *J Mater Chem C Mater*, 2022, **10**, 16949–16982.

44 M. H. Tremblay, J. Bacsa, B. Zhao, F. Pulvirenti, S. Barlow and S. R. Marder, *Chemistry of Materials*, 2019, **31**, 6145–6153.

45 G. Lv, L. Li, D. Lu, Z. Xu, Y. Dong, Q. Li, Z. Chang, W. J. Yin and Y. Liu, *Nano Lett*, 2021, **21**, 5788–5797.

46 J. Shi, Y. Gao, X. Gao, Y. Zhang, J. Zhang, X. Jing, M. Shao, J. Shi, Y. Gao, Y. Zhang, J. Zhang, X. Jing, M. Shao and X. Gao, *Advanced Materials*, 2019, **31**, 1901673.

47 Q. Li, Y. Dong, G. Lv, T. Liu, D. Lu, N. Zheng, X. Dong, Z. Xu, Z. Xie and Y. Liu, *ACS Energy Lett*, 2021, **6**, 2072–2080.

48 H. Pan, X. Zhao, X. Gong, Y. Shen and M. Wang, *Journal of Physical Chemistry Letters*, 2019, **10**, 1813–1819.

49 Y. Jiang, M. Cui, S. Li, C. Sun, Y. Huang, J. Wei, L. Zhang, M. Lv, C. Qin, Y. Liu and M. Yuan, *Nature Communications 2021 12:1*, 2021, **12**, 1–10.

50 N. Li, S. Tao, Y. Chen, X. Niu, C. K. Onwudinanti, C. Hu, Z. Qiu, Z. Xu, G. Zheng, L. Wang, Y. Zhang, L. Li, H. Liu, Y. Lun, J. Hong, X. Wang, Y. Liu, H. Xie, Y. Gao, Y. Bai, S. Yang, G. Brocks, Q. Chen and H. Zhou, *Nature Energy 2019 4:5*, 2019, **4**, 408–415.

51 W. M. Gu, Y. Zhang, K. J. Jiang, G. Yu, Y. Xu, J. H. Huang, Y. Zhang, F. Wang, Y. Li, Y. Lin, X. Jiao, C. Y. Gao, H. Fan, N. Wu, X. Zhou and Y. Song, *J Mater Chem A Mater*, 2022, **10**, 12882–12889.

52 H. Tsai, D. Ghosh, W. Panaccione, L. Y. Su, C. H. Hou, L. Wang, L. R. Cao, S. Tretiak and W. Nie, *ACS Energy Lett*, 2022, 3871–3879.

53 W. Fu, H. Liu, X. Shi, L. Zuo, X. Li and A. K. Y. Jen, *Adv Funct Mater*, 2019, **29**, 1900221.

54 C. Mora Perez, D. Ghosh, O. Prezhdo, W. Nie, S. Tretiak and A. Neukirch, *J Phys Chem Lett*, 2022, **13**, 5213–5219.

55 D. Ghosh, A. J. Neukirch and S. Tretiak, *J Phys Chem Lett*, 2020, **11**, 2955–2964.

56 D. Ghosh, C. M. Perez, O. Prezhdo, W. Nie, S. Tretiak and A. J. Neukirch, *J Mater Chem C Mater*, 2022, **10**, 9563–9572.

57 H. Tsai, D. Ghosh, E. Kinigstein, B. Dryzhakov, H. Driscoll, M. Owczarek, B. Hu, X. Zhang, S. Tretiak and W. Nie, *Nano Lett*, , DOI:10.1021/acs.nanolett.2c03403.

58 P. P. Shi, S. Q. Lu, X. J. Song, X. G. Chen, W. Q. Liao, P. F. Li, Y. Y. Tang and R. G. Xiong, *J Am Chem Soc*, 2019, **141**, 18334–18340.

59 E. R. Johnson, S. Keinan, P. Mori-Sánchez, J. Contreras-García, A. J. Cohen and W. Yang, *J Am Chem Soc*, 2010, **132**, 6498–6506.

60 J. Contreras-García, E. R. Johnson, S. Keinan, R. Chaudret, J. P. Piquemal, D. N. Beratan and W. Yang, *J Chem Theory Comput*, 2011, **7**, 625–632.

61 F. El-Mellouhi, S. N. Rashkeev, A. Marzouk, L. Kabalan, A. Belaidi, B. Merzougui, N. Tabet and F. H. Alharbi, *J Mater Chem C Mater*, 2019, **7**, 5299–5306.

62 J.-H. Lee, N. C. Bristowe, J. Ho Lee, S.-H. Lee, P. D. Bristowe, A. K. Cheetham and H. Myung Jang, *Chemistry of Materials*, 2016, **28**, 4259–4266.

63 D. Ghosh, A. R. Smith, A. B. Walker and M. Saiful Islam, *Chemistry of Materials*, 2018, **30**, 5194–5204.

64 G. Cavallo, P. Metrangolo, R. Milani, T. Pilati, A. Priimagi, G. Resnati and G. Terraneo, *Chem Rev*, 2016, 116, 2478–2601.

65 H. Tsai, D. Ghosh, W. Panaccione, L.-Y. Su, C.-H. Hou, L. Wang, L. Raymond Cao, S. Tretiak and W. Nie, *ACS Energy Lett*, 2022, **7**, 3871–3879.

66 Z. Wang, Q. Wei, X. Liu, L. Liu, X. Tang, J. Guo, S. Ren, G. Xing, D. Zhao and Y. Zheng, *Adv Funct Mater*, 2021, **31**, 2008404.

67 L. Mao, W. Ke, L. Pedesseau, Y. Wu, C. Katan, J. Even, M. R. Wasielewski, C. C. Stoumpos and M. G. Kanatzidis, *J Am Chem Soc*, 2018, **140**, 3775–3783.

68 Q. Zhou, Q. Xiong, Z. Zhang, J. Hu, F. Lin, L. Liang, T. Wu, X. Wang, J. Wu, B. Zhang and P. Gao, *Solar RRL*, 2020, **4**, 2000107.

69 E. Mosconi, A. A. Alothman, R. Long, W. Kaiser and F. de Angelis, *ACS Energy Lett*, 2022, **8**, 748–752.

70 J. H. Lee, J. H. Lee, E. H. Kong and H. M. Jang, *Scientific Reports 2016 6:1*, 2016, **6**, 1–12.

71 S.-F. Zhang, X.-K. Chen, A.-M. Ren, H. Li and J.-L. Bredas, *ACS Energy Lett*, 2018, **4**, 17–25.

72 D. Dai, R. Shi and R. Long, *J Phys Chem Lett*, 2022, **13**, 2718–2724.

73 X. Gong, O. Voznyy, A. Jain, W. Liu, R. Sabatini, Z. Piontkowski, G. Walters, G. Bappi, S. Nokhrin, O. Bushuyev, M. Yuan, R. Comin, D. McCamant, S. O. Kelley and E. H. Sargent, *Nat Mater*, 2018, **17**, 550–556.

74 D. Ghosh, A. Aziz, J. A. Dawson, A. B. Walker and M. Saiful Islam, *Chemistry of Materials*, 2019, **31**, 4063–4071.

75 M. R. Filip, G. E. Eperon, H. J. Snaith and F. Giustino, *Nature Communications 2014 5:1*, 2014, **5**, 1–9.

76 A. A. Koegel, E. M. Mozur, I. W. H. Oswald, N. H. Jalarvo, T. R. Prisk, M. Tyagi and J. R. Neilson, *J Am Chem Soc*, 2022, **144**, 1313–1322.

77 M. Z. Mayers, L. Z. Tan, D. A. Egger, A. M. Rappe and D. R. Reichman, *Nano Lett*, 2018, **18**, 8041–8046.

78 W. Li, Y. She, A. S. Vasenko and O. v. Prezhdo, *Nanoscale*, 2021, 13, 10239–10265.

79 L. Li and E. A. Carter, *J Am Chem Soc*, 2019, **141**, 10451–10461.

80 S. F. Zhang, X. K. Chen, A. M. Ren, H. Li and J. L. Bredas, *ACS Energy Lett*, 2019, **4**, 17–25.

81 X. Li, W. Ke, B. Traoré, P. Guo, I. Hadar, M. Kepenekian, J. Even, C. Katan, C. C. Stoumpos, R. D. Schaller and M. G. Kanatzidis, *J Am Chem Soc*, 2019, **141**, 12880–12890.

82 Y. Lei, Y. Li, C. Lu, Q. Yan, Y. Wu, F. Babbe, H. Gong, S. Zhang, J. Zhou, R. Wang, R. Zhang, Y. Chen, H. Tsai, Y. Gu, H. Hu, Y. H. Lo, W. Nie, T. Lee, J. Luo, K. Yang, K. I. Jang and S. Xu, *Nature*, 2022, **608**, 317–323.

83 P. Fu, M. A. Quintero, C. Welton, X. Li, B. Cucco, M. C. De Siena, J. Even, G. Volonakis, M. Kepenekian, R. Liu, C. C. Laing, V. Klepov, Y. Liu, V. P. Dravid, G. N. Manjunatha Reddy, C. Li and M. G. Kanatzidis, *Chemistry of Materials*, 2022, **34**, 9685–9698.

84 R. Shi, Q. Fang, A. S. Vasenko, R. Long, W. H. Fang and O. v. Prezhdo, *J Am Chem Soc*, 2022, **144**, 19137–19149.

85 O. v. Prezhdo, *Acc Chem Res*, 2021, **54**, 4239–4249.

86 A. Biewald, N. Giesbrecht, T. Bein, P. Docampo, A. Hartschuh and R. Ciesielski, *ACS Appl Mater Interfaces*, 2019, **11**, 20838–20844.

87 A. D. Wright, C. Verdi, R. L. Milot, G. E. Eperon, M. A. Pérez-Osorio, H. J. Snaith, F. Giustino, M. B. Johnston and L. M. Herz, *Nature Communications 2016 7:1*, 2016, **7**, 1–9.

88 A. J. Neukirch, K. Hyeon-Deuk and O. v. Prezhdo, *Coord Chem Rev*, 2014, 263–264, 161–181.

89 A. v. Akimov and O. v. Prezhdo, *J Chem Theory Comput*, 2013, **9**, 4959–4972.

90 C. F. Craig, W. R. Duncan and O. v. Prezhdo, *Phys Rev Lett*, 2005, **95**, 163001.

91 R. Long, J. Liu and O. v. Prezhdo, *J Am Chem Soc*, 2016, **138**, 3884–3890.

92 D. Dai, R. Shi and R. Long, *Journal of Physical Chemistry Letters*, 2022, **13**, 2718–2724.

93 A. Nijamudheen and A. v. Akimov, *Journal of Physical Chemistry Letters*, 2018, **9**, 248–257.

94 Z. Zhang, W. H. Fang, R. Long and O. v. Prezhdo, *J Am Chem Soc*, 2019, **141**, 15557–15566.

95 B. Dhanabalan, Y.-C. Leng, G. Biffi, M.-L. Lin, P.-H. Tan, I. Infante, L. Manna, M. P. Arciniegas and R. Krahne, *ACS Nano*, 2020, **14**, 4689–4697.

96 Z. Zhang, W.-H. Fang, R. Long and O. v. Prezhdo, *J Am Chem Soc*, 2019, **141**, 15557–15566.

97 M. A. Pérez-Osorio, R. L. Milot, M. R. Filip, J. B. Patel, L. M. Herz, M. B. Johnston and F. Giustino, *The Journal of Physical Chemistry C*, 2015, **119**, 25703–25718.

98 Y. Wang, L. Pedesseau, C. Katan, J. Even, O. v. Prezhdo, S. Tretiak, D. Ghosh and A. J. Neukirch, *Appl Phys Lett*, 2021, **119**, 201102.

99 A. J. Neukirch, K. Hyeon-Deuk and O. v. Prezhdo, *Coord Chem Rev*, 2014, 263–264, 161–181.

100 A. v. Akimov, R. Long and O. v. Prezhdo, *J Chem Phys*, 2014, **140**, 194107.

101 S. v. Kilina, A. J. Neukirch, B. F. Habenicht, D. S. Kilin and O. v. Prezhdo, *Phys Rev Lett*, 2013, **110**, 180404.

102 A. B. Madrid, K. Hyeon-Deuk, B. F. Habenicht and O. v. Prezhdo, *ACS Nano*, 2009, **3**, 2487–2494.

103 O. v. Prezhdo and P. J. Rossky, *Phys Rev Lett*, 1998, **81**, 5294.

104 R. Englman and J. Jortner, *J Lumin*, 1970, **1–2**, 134–142.

105 R. Long, O. v. Prezhdo and W. Fang, *Wiley Interdiscip Rev Comput Mol Sci*, 2017, **7**, e1305.

106 G. Kresse and J. Hafner, *Phys Rev B*, 1993, **47**, 558.

107 G. Kresse and J. Hafner, *Phys Rev B*, 1994, **49**, 14251.

108 G. Kresse and J. Furthmüller, *Phys Rev B*, 1996, **54**, 11169.

109 G. Kresse and D. Joubert, *Phys Rev B*, 1999, **59**, 1758.

110 J. P. Perdew, K. Burke and M. Ernzerhof, *Phys Rev Lett*, 1996, **77**, 3865.

111 S. Grimme, J. Antony, S. Ehrlich and H. Krieg, *J Chem Phys*, 2010, **132**, 154104.

112 H. J. Monkhorst and J. D. Pack, *Phys Rev B*, 1976, **13**, 5188.

113 K. Momma and F. Izumi, *J Appl Crystallogr*, 2011, **44**, 1272–1276.

114 H. M. Jaeger, S. Fischer and O. v. Prezhdo, *J Chem Phys*, 2012, **137**, 22A545.

115 W. Li, R. Long, J. Tang and O. v. Prezhdo, *Journal of Physical Chemistry Letters*, 2019, **10**, 3788–3804.

116 B. G. Janesko, *Chem Soc Rev*, 2021, **50**, 8470–8495.

117 R. Shinde, S. S. R. K. C. Yamijala and B. M. Wong, *Journal of Physics: Condensed Matter*, 2020, **33**, 115501.

118 T. Tsuneda and K. Hirao, *J Chem Phys*, 2014, **140**, 18A513.

119 A. v. Akimov and O. v. Prezhdo, *J Chem Theory Comput*, 2013, **9**, 4959–4972.

120 A. v. Akimov and O. v. Prezhdo, *J Chem Theory Comput*, 2014, **10**, 789–804.

121 P. Hamm, *Principles of Nonlinear Optical Spectroscopy: A Practical Approach or: Mukamel for Dummies*, 2005.

122 A. v. Akimov and O. v. Prezhdo, *Journal of Physical Chemistry Letters*, 2013, **4**, 3857–3864.

123 P. Hamm, *Principles of Nonlinear Optical Spectroscopy: A Practical Approach or: Mukamel for Dummies*, University of Zurich, 2005, vol. 41.

124 W. Li, L. Zhou, O. v. Prezhdo and A. v. Akimov, *ACS Energy Lett*, 2018, **3**, 2159–2166.